

**Kinetics of Furfural Electrochemical Hydrogenation and Hydrogenolysis in Acidic Media on Copper**

Journal:	<i>Reaction Chemistry &amp; Engineering</i>
Manuscript ID	RE-ART-06-2021-000216.R1
Article Type:	Paper
Date Submitted by the Author:	12-Aug-2021
Complete List of Authors:	May, Andrew; The City College of New York, CUNY, Chemical Engineering Watt, Steven; The City College of New York, CUNY, Chemical Engineering; The Graduate Center of the City University of New York, Ph.D. Program in Chemistry Biddinger, Elizabeth; The City College of New York, CUNY, Chemical Engineering; The Graduate Center of the City University of New York, Ph.D. Program in Chemistry

## Kinetics of Furfural Electrochemical Hydrogenation and Hydrogenolysis in Acidic Media on Copper

Andrew S. May<sup>1</sup>, Steven M. Watt<sup>1,2</sup>, and Elizabeth J. Biddinger<sup>1,2\*</sup>

<sup>1</sup>Department of Chemical Engineering, The City College of New York, CUNY, New York, New York 10031, United States

<sup>2</sup>Ph.D. Program in Chemistry, The Graduate Center of the City University of New York, New York, New York 10016, United States

\* [ebiddinger@ccny.cuny.edu](mailto:ebiddinger@ccny.cuny.edu)

**Keywords:** Electrochemical, hydrogenation, hydrogenolysis, biomass, kinetics, green energy, furfural, Langmuir-Hinshelwood, Eley-Rideal, mechanism

### Abstract:

Electrochemical processes can be implemented for the valorization of biomass-derived species such as furfural to generate fine chemicals and fuels. The electrochemical hydrogenation and hydrogenolysis (ECH) of furfural (FF) can produce furfuryl alcohol (FA) and 2-methylfuran (MF) as the major products over Cu catalysts in acidic conditions. The production of these species are in competition and the kinetics of these reactions should be studied so that the product distribution can be better controlled. In this work, the competing kinetics of furfural ECH to furfuryl alcohol and 2-methylfuran were studied on Cu in acidic media by using the applied cathodic potential, temperature, and initial concentration of furfural as probes. An increased temperature of the system was shown to promote the MF production in the range tested (15°C and 45°C), however the production of FA was decreased when the temperature was increased from 35°C to 45°C, due to significant promotion of side reactions. By varying the concentration of FF used in bulk electrolysis, we saw that the rates of reaction to FA and MF shift from positive order to zero order, suggesting a Langmuir-Hinshelwood or Eley-Rideal mechanism at -0.56 V vs. RHE and 25°C. An analysis of the reaction mechanisms showed that a non-competitive Langmuir-Hinshelwood mechanism is likely occurring. In addition, we suggest the likely rate limiting steps based on mechanisms are the first hydrogenation step of FF to  $C_4H_3O-CH_2O$  to form FA, and the C-O cleavage of the  $C_4H_3O-CHOH$  intermediate to form MF.

### Introduction:

The development of renewable processes that can replace or lessen the dependence on petroleum feedstocks has become a growing area of focus. These processes require a feedstock that is renewable on a much shorter timescale than fossil fuels, such as biomass, which provides the carbon source for fuels and chemicals. Biomass can be used to produce a bio-oil via fast pyrolysis with yields up to 70%<sup>1</sup>. Bio-oil contains greater than 300 molecules and requires chemical upgrading to biofuels and value-added products. Traditional upgrading is by way of hydrotreatment<sup>2</sup>, however the bio-oil will more rapidly polymerize at temperatures above 80°C which is required in this process<sup>3, 4</sup>. An alternative process is electrochemical hydrogenation and hydrogenolysis (ECH)<sup>3-8</sup>. The electrochemical methods do not require an external supply of hydrogen gas, as protons for reaction are generated in-situ from the electrolyte. Hydrogen gas is largely produced via steam reforming which has high CO<sub>2</sub> emissions. Electrochemical upgrading can also operate at room temperature to avoid high temperatures that cause polymerization. The energy driving the reaction is in the form of electricity, so it can be efficiently coupled to renewable electricity.

To gain a better understanding of the mechanisms of ECH on bio-oil compounds, individual or small classes of species need to be studied. One molecule of interest present in bio-oils is furfural (FF), which has been identified as a top 30 biomass-derived building block chemical for its abundance, cost, and significance to the future of biorefinery processes<sup>9</sup>. In addition to being found in bio-oil, FF is a bioproduct produced at scale from pentosan-rich agricultural materials via the Quaker process<sup>10</sup>, which could allow for the unique opportunity to pursue electrochemical hydrogenation systems for a FF rich feedstock while gaining insights to the broader bio-oil processes. The FF ECH products of interest are 2-methylfuran (MF), proposed as a high-octane fuel or fuel additive<sup>11</sup>, and furfuryl alcohol (FA), which is used in the production of binders and polymers<sup>12</sup>. The electroreduction of FF was first recorded in 1939 by Albert and Lowy who achieved a 63% yield on Pb electrodes to the dimer product hydrofuroin, a rocket fuel precursor, in addition to small amounts of FA and a resin product<sup>13</sup>. More recently, the FF ECH process has been studied by manipulation of reaction parameters, including: catalyst<sup>14-23</sup>, electrolyte<sup>16, 22-25</sup>, electrode potential<sup>15, 23, 26, 27</sup>, and temperature<sup>15</sup>, resulting in a variety of selectivities towards MF and FA, with typically very low-to-no selectivities towards hydrofuroin. Notably, the highest selectivity of MF, nearing 80%, was achieved by Nilges and Schröder over Cu catalysts in acidic electrolyte<sup>14</sup>. Cu catalysts have a moderate hydrogen overpotential<sup>28</sup> which is useful to limit the competing hydrogen evolution reaction (HER) reaction yet still have hydrogen adsorb on the surface. Additionally, Cu benefits from its availability<sup>29, 30</sup> and its low

cost<sup>31, 32</sup>, however stability issues compared to noble metals have been reported<sup>18</sup>. Thus, Cu is a metal of interest in the field for FF ECH. In our group we have investigated FF ECH over Cu catalyst in acidic conditions<sup>21, 25, 27</sup> so that we can intentionally study the competing reactions between FA and MF. We have shown that low pH strongly drives the reaction selectivity towards MF<sup>25</sup>, that acetonitrile co-solvent in volume ratios of 20:80 to 80:20 mitigate competing homogenous side reactions of furanics<sup>25</sup>, and that high overpotentials lead to lower faradaic efficiencies for ECH due to the increase in rate of HER<sup>27</sup>. Additionally, we have shown that ECH of FA and MF likely occur in parallel reactions as when a cathodic potential was applied to just FA as the reactant, a negligible amount of MF was detected<sup>27</sup>.

While studies of the effect of reaction parameters on reaction efficiency and selectivity towards products are important for reaction optimization, studies on the fundamental mechanism and kinetics of ECH of FF are required to understand the observed trends. Liu et al. showed that in basic electrolyte (pH 10), the rate-limiting step of ECH of FF over Cu was the generation of a carbon-free radical by a solution proton and electron from the catalyst<sup>33</sup>. Chadderdon et al. concluded that for ECH of FF over Cu in acidic electrolyte, the first reaction step involved electrons at the cathode surface and protons from solution, followed by reaction of the carbon radical with adsorbed hydrogen to produce FA and MF in parallel reactions<sup>23</sup>.

The kinetics of the parallel ECH reactions to FA and MF must be understood so that processes can selectively target the desired product and simultaneously achieve high rates of production. This work investigates the relationship between the production rates of FA and MF by probing the potential, concentration of FF, and temperature of the reactions. In this work, both the FA and MF products were produced, while no dimer product was detected in any experiments and so will not be discussed further. Experiments are done in acidic conditions over Cu so that both products are formed and the competition between the two can be studied. We show in this work how the probe variables impact the competition between FA and MF production from FF ECH. In addition, by developing mechanistic models based on different possible reaction pathways, we were able to provide insights into the mechanisms of the FF ECH reactions by showing which models provide strong fits.

### **Experimental:**

**Materials:** For bulk electrolysis experiments, Cu electrode flags were made from Cu foil (99.999%) 0.1 mm thickness from Alfa Aesar and Cu wire (99.999%) 0.5mm diameter from Alfa Aesar. A Pt gauze flag was made from Pt gauze (99.9%) 0.1 mm thickness 52 mesh welded

onto Pt wire (99.95%) 0.5 mm diameter. A silver/silver chloride (Ag/AgCl) 3 M sodium chloride reference electrode MR-5275 from BASi was used. Gas sparging was done with N<sub>2</sub> (5.0 ultra high purity, Praxair) or 4 mol% H<sub>2</sub> in Ar gas (Praxair). DI water for solution preparation was 18.2 MΩ•cm and was obtained from the lab Millipore system (Milli-Q Direct 8 Water Purification System). Acetonitrile (optima grade, Fisher), acetone (optima grade Fisher), chloroform with ethanol as stabilizer (HPLC grade, Beantown Chemical), furfural (99% Sigma-Aldrich), furfuryl alcohol (98% Acros), 2-methylfuran (99% with BHT as stabilizer, Sigma), sulfuric acid (93%-98% trace metal grade, Fisher), sodium chloride (Acros), and sodium sulfate anhydrous (Fisher) were all used without further treatment. Hydrochloric acid (37%, Fisher) was diluted to 10 vol% in DI water.

**Electrochemical Cell Setup:** The electrode preparation was as follows: The electrode was first constructed using Cu foil and Cu wire to make a flag of 2 cm by 1.5 cm foil surface (per side). The electrode was then submerged into acetone and sonicated for 10 minutes. It was rinsed with DI water, submerged into 10 vol% hydrochloric acid for 1 minute to remove any oxidation on the surface, and rinsed with DI water again before use.

The electrochemical cell consisted of a 2 compartment H-type cell separated by a Nafion 117 membrane and with a solvent trap connected to the catholyte chamber. The anolyte was 30 mL of 0.1 M or 0.5 M sulfuric acid. The catholyte was 35 mL of a solution of 20 vol% acetonitrile and 80 vol% water, with 0.1 M or 0.5 M sulfuric acid and 10-120 mM of FF. The solvent trap was 60 mL of acetonitrile in a glass tube with a sample port which was then placed into a bath containing a mix of ice and salt to reach -15°C. The anolyte chamber had a Pt gauze counter electrode, and the catholyte chamber contained the Cu working electrode, Ag/AgCl reference electrode, and a gas line to bubble N<sub>2</sub> at 60 mL/min, as well as a stir bar set to rotate at 600 RPM via magnetic stirrer hotplate. Additionally, the catholyte chamber was capped so that the flow of N<sub>2</sub>, H<sub>2</sub> and volatiles would travel into the solvent trap. The H-cell was placed into a water bath to maintain the desired temperature throughout the experiment.

For bulk electrolysis, chronoamperometry was run using a Gamry Interface 1000 potentiostat. The potential was set between -0.485 and -0.645 V vs RHE for 30 minutes. The working electrode was positioned 4 mm away from the reference electrode, and the uncompensated resistance (Ru) of the cell was measured. Chronoamperometry was run with 100% of iR correction done post experiment manually. The following equation is used to convert from Ag/AgCl to RHE, noting that  $E_{\text{Ag/AgCl}}^0$  is temperature dependent and is input per table S1:

$$E_{RHE} = E_{Ag/AgCl} + 0.059 \text{ pH} + E_{Ag/AgCl}^0 \quad (1)$$

The temperature and potential were 25°C and -0.56 V vs RHE for experiments where the temperature or potential were not the parameter being studied, as these values were selected to have high rates to desired products while limiting HER and homogeneous side reactions.

**Analysis.** Samples of 0.5 mL from catholyte and solvent trap were taken by syringe through a rubber septum. The catholyte samples were placed into small vials containing 150 mg sodium chloride, and the solvent trap samples were placed into empty vials. Calculations take into consideration the slight change in volume and consumption of furanics due to sampling, however, to avoid complication, the equations are written in the simplest form.

The workup of samples was done to remove the aqueous phase of the catholyte sample so that it could be analyzed by gas chromatographer mass spectrometer (GCMS). 2 mL of 0°C chloroform was added to the sample vial, and the sample was capped and shaken. After a short amount of time, the sample solution would phase separate, and the organic phase was extracted by syringe. Next, the organic phase was added into a separate vial containing 100 mg of Na<sub>2</sub>SO<sub>4</sub> to further dehydrate the sample. The solution was passed through a 25 µm syringe filter and placed into a GC vial for analysis. Solvent trap samples were diluted by adding 1mL of acetonitrile. Calibration curves relating the peak area from the GCMS to the concentration of furanics in injected solution were constructed to calculate the concentration of samples from the catholyte and solvent trap.

A GCMS (QP 2010 Ultra, Shimadzu), which contained a TR-WAXMS column (length = 30 m, diameter = 0.25 mm, thickness = 0.25 µm, Thermo Scientific) was used for analysis of samples.

All error bars shown are the standard deviation from experiments done in at least duplicate.

### Curve fittings:

MATLAB version R2020a was used to assist in curve fitting of derived models. The built-in function `lsqcurvefit` generated the rate constants by the non-linear least squares for the set of two equations derived (MF and FA). The built-in function `nlparci` generated the rate constant 95% confidence intervals. Reduced chi-squared values were calculated for the FA and MF rate equations for each model.

**Calculations:**

Conversion:

$$X_{FF} = \frac{[FF]_i - [FF]_t}{[FF]_i} * 100\% \quad (2)$$

Where  $X_{FF}$  is conversion of FF,  $[FF]_i$  the initial concentration of FF, and  $[FF]_t$  is the concentration of FF at time t.

Selectivity:

$$S_{FA} = \frac{[FA]_t}{[FF]_i - [FF]_t} * 100\% \quad (3)$$

$$S_{MF} = \frac{[MF]_t}{[FF]_i - [FF]_t} * 100\% \quad (4)$$

Where  $S_{FA}$  is the selectivity to FA,  $S_{MF}$  is the selectivity to MF,  $[FA]_t$  is the concentration of FA at time t, and  $[MF]_t$  is the concentration of MF at time t.

Yield:

$$Y_{FA} = \frac{[FA]_t}{[FF]_i} * 100\% \quad (5)$$

$$Y_{MF} = \frac{[MF]_t}{[FF]_i} * 100\% \quad (6)$$

Where  $Y_{FA}$  is the yield of FA, and  $Y_{MF}$  is the yield of MF.

Faradaic Efficiency:

$$FE_{FA} = \frac{n_{FA} * F * z}{\int I dt} * 100\% \quad (7)$$

$$FE_{MF} = \frac{n_{MF} * F * z}{\int I dt} * 100\% \quad (8)$$

Where F is the Faraday constant (96485 C/mol),  $FE_{FA}$  is the Faradaic efficiency to FA,  $n_{FA}$  is the amount of FA in mmol,  $FE_{MF}$  is the Faradaic efficiency to MF,  $n_{MF}$  is the amount of MF in mmol, z is the number of electrons reacted (2 for FA and 4 for MF), I is the current in mA, and t is time in seconds.

Mole Balance:

$$MB = \frac{([FF]_t + [FA]_t + [MF]_t)}{[FF]_i} * 100\% \quad (9)$$

Where MB is the mole balance closure.

Production rate:

$$Rate_{FA} = \frac{[FA]_{t_i} - [FA]_{t_{i-1}}}{(t_i - t_{i-1})} \quad (10)$$

$$Rate_{MF} = \frac{[MF]_{t_i} - [MF]_{t_{i-1}}}{(t_i - t_{i-1})} \quad (11)$$

Where  $Rate_{FA}$  is the rate of production of FA,  $Rate_{MF}$  is the rate of production of MF,  $t_i$  is the time of the sample of interest,  $t_{i-1}$  is the time of the sample before the sample of interest,  $[FA]_{t_i}$  is the concentration of FA at  $t_i$ ,  $[FA]_{t_{i-1}}$  is the concentration of FA at  $t_{i-1}$ ,  $[MF]_{t_i}$  the concentration of MF at  $t_i$  and  $[MF]_{t_{i-1}}$  is the concentration of MF at  $t_{i-1}$ .

**Partial Current Density:**

$$j_{FA} = \frac{n_{FA}}{1000 \left(\frac{mmol}{mol}\right)} * NA * 2 e^- * q_e * \frac{1}{t} \quad (12)$$

$$j_{MF} = \frac{n_{MF}}{1000 \left(\frac{mmol}{mol}\right)} * NA * 4 e^- * q_e * \frac{1}{t} \quad (13)$$

Where  $j_{FA}$  is the partial current density for FA,  $j_{MF}$  is the partial current density for MF, NA is Avagadro's number, and  $q_e$  is the charge of an electron.

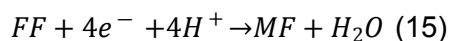
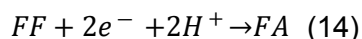
**Results and Discussion:**

**Impact of Applied Potential:**

The use of acidic electrolyte enables the production of MF, which has been observed below pH 3.4 over Cu electrodes<sup>8, 14, 21, 23, 25-27</sup>. In this work we studied the parallel reactions towards FA and MF in acidic conditions over Cu electrodes to capture the competing kinetics. To study the kinetics, a system that is not limited by mass transfer is required. This is dependent on factors such as the applied potential and convection from stirring and N<sub>2</sub> sparging. In our system, with stirring at 600 RPM, a mass transfer limited regime was not reached until potentials exceeding -0.6V were applied at the cathode, signified by the onset of a plateau current. Mass transfer was investigated in 0.5M H<sub>2</sub>SO<sub>4</sub> with 100mM FF with control tests with different stir rates and

presence of gas bubbling. Compared to a control with no stirring or gas bubbling, the current increased by 50% with the addition of either gas sparging at 60mL/min or 600 RPM stirring with a magnetic stir bar. No further current increase was found by stirring at 600RPM while sparging gas, and no further current increase was found by increasing the stir rate to 900 RPM. Figure S1 shows the conversion of FF with different forced convection, we found that further increases to stir rate do not impact the conversion of FF.

The ECH of FF at an initial concentration of 100 mM was studied at applied potentials between -0.485 V vs RHE and -0.645 V vs RHE with 0.5 M H<sub>2</sub>SO<sub>4</sub> (pH 0) electrolyte, and the resulting partial current densities towards FA and MF production are shown in Figure 1a. In the range of -0.517 V to -0.572 V vs RHE, an exponential growth was observed for partial current density towards both FA and MF, showing Butler-Volmer kinetics within this range. Further increases to the overpotential showed a plateau in current density of both products, indicating a mass-transfer limited regime. The partial current density towards MF in the exponential region of the graph was on average 3.9 times larger than that towards FA, which corresponded to a 1.9 times larger production rate because MF production requires 4 electrons while FA production requires 2 electrons per FF. This can be seen in the overall reactions:



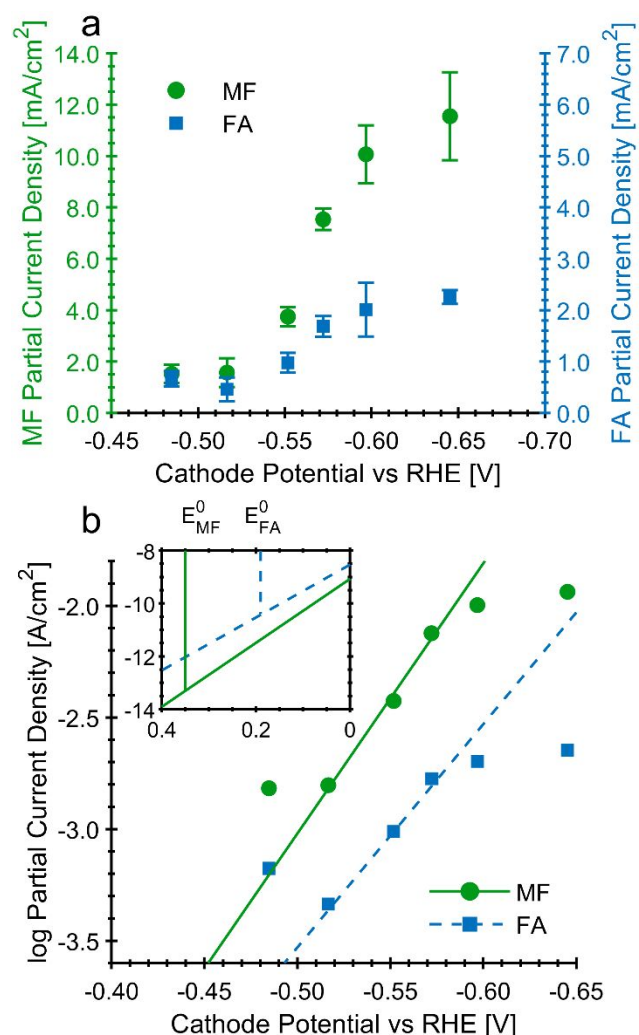


Figure 1. (a) Potential dependence of partial current densities of FF to FA and MF. (b) Tafel plot for the ECH of FF to FA and MF. The standard potentials are marked on the inset at 0.192V and 0.352V and labeled  $E_{FA}^0$  and  $E_{MF}^0$ . Conditions: 100 mM FF initial concentration, 25°C, 80:20 v:v DI water to acetonitrile with 0.5 M sulfuric acid. Average current density and Faradaic efficiency after 30 minutes of ECH can be found in Table S2.

The logarithm of current density showed a linear fit between -0.517 V and -0.572 V vs RHE for both FA and MF. The Tafel slopes were found to be 0.0827 and 0.0996 V/decade for FA and MF, respectively. The corresponding current found by extrapolation of the Tafel fit to the standard reaction potentials, labeled in the inset of Figure 1b as 0.192 V and 0.352 V for FF ECH to FA and MF, gave the exchange current densities. The exchange current densities were

found to be  $3.50 \times 10^{-11} \text{ A cm}^{-2}$  and  $4.76 \times 10^{-14} \text{ A cm}^{-2}$  for FF ECH to FA and MF, respectively. The Tafel slopes are useful to give insights into the rate determining steps of the mechanism and exchange current densities are useful in comparing activity or catalysts for the reactions of interest<sup>34</sup>. The Tafel slope has commonly been used for reactions such as HER to give insights into the rate limiting step, however it cannot provide definitive evidence alone<sup>34</sup>. The exchange current density of MF was much lower than that of FA showing that the kinetics of MF were more sluggish than that of FA. Since MF has a more positive standard potential, when a reduction reaction is run at conditions tested in this work the overpotential for the MF reaction is larger which leads to the reaction rate exceeded that of the FA reaction. The Tafel slopes are similar in the reactions of FF to FA and FF to MF, which could suggest that the reactions both occur either via 1-electron step rate limiting reactions, or 2 electron rate limiting step reactions, assuming the symmetry factors to be identical. This can be helpful in determining the mechanism of the competing reactions.

As a control experiment, 4% $\text{H}_2$ /Ar gas was sparged into the H-cell, replacing the  $\text{N}_2$  gas, to determine if hydrogen gas generated in-situ during electrolysis was the cause of FA and MF formation through a thermochemical hydrogenation or hydrogenolysis route. After 90 minutes of electrolysis with the 4% $\text{H}_2$ /Ar gas sparged at 60mL/min, no conversion of FF was seen, and no FA or MF was found. This result shows that the formation of FA and MF from FF is due to the applied potential. The concentrations of FF, FA, and MF over time with 4% $\text{H}_2$ /Ar gas can be seen in Figure S2.

### **Impact of Temperature:**

The effect of temperature on the conversion, mole balance, selectivity, and faradaic efficiency was studied between 15°C and 45°C at -0.56 V vs. RHE in 0.5M  $\text{H}_2\text{SO}_4$ . This potential was selected to allow for a high rate towards ECH without having mass transfer limitations. Higher temperatures led to increased conversion at 30 minutes of electrolysis due to the increased rate of reaction. The mass balance closure had an inverse relationship with temperature, displayed in Figure 2a. In addition, the catholyte after experimentation showed a dark orange color in the electrolyte along with residue build-up on the reactor walls for the 35°C and 45°C temperature test while the 15°C temperature test showed no visible change from the pre-ECH, shown in Figure S3.

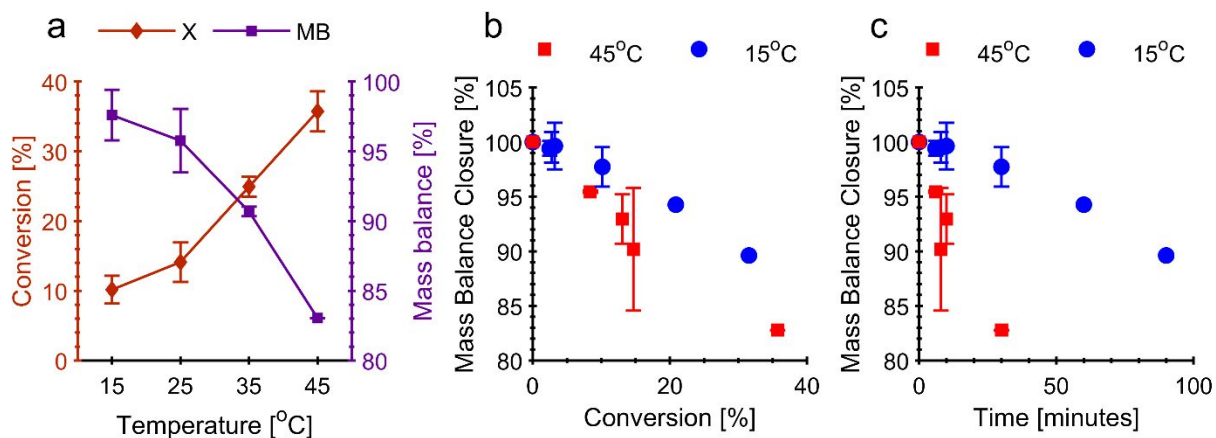


Figure 2. (a) The conversion of FF and mass balance of the system of ECH of FF between 15°C and 45°C at 30 minutes of ECH. Mass balance closure as a function of the (b) conversion and (c) time for ECH of FF at 15°C and 45°C until 90 minutes of ECH. Conditions: 100 mM FF initial concentration, -0.560 V vs RHE, 80:20 v:v DI water to acetonitrile with 0.5 M H<sub>2</sub>SO<sub>4</sub>.

To investigate further which compound was responsible for the color change, three vials were prepared: 1) 100mM FF, 2) 25mM FA, and 3) a mix of 100mM FF with 25mM FA all in 0.5M H<sub>2</sub>SO<sub>4</sub> with a 80:20 ratio of water to acetonitrile were placed into a water bath at 45°C. The vials were sampled before and after 30 minutes spent in the water bath. MF was not investigated as it transfers from the catholyte to the solvent trap where it is primarily collected. Both vials containing FA became a similar orange color as observed during ECH at 45°C, shown in Figure S4. The vial containing only FF did not change color noticeably. The vial containing both FF and FA was noticeably darker than the vial containing FA and no FF, however analysis showed that it was likely not due to a reaction of FF with FA as in both vials containing FF the drop in FF concentration was negligible (0% and 1%). The homogeneous reactions were identified as being due to FA, as the drop FA concentration for vials with and without FF were 61% and 60%, respectively. Additionally, neither FA or MF was not detected in the FF vial after 30 minutes spent in the water bath, nor was MF detected in either vial containing FA after 30 minutes spent in the water bath. Our group's previous works have shown the negative impact of homogeneous side reactions on the selectivity of desired products<sup>25, 27</sup>. The current work showed that the homogeneous side reactions are temperature dependant which led to the inverse relationship between mass balance and temperature.

To discern whether the effect on the mole balance was due to the change in temperature or degree of conversion, electrolysis was run at 15°C for 90 minutes, until the conversion at 15°C was comparable to the 45°C test. Figure 2b shows the conversion plotted against the mass balance for electrolysis at 15°C and 45°C.

When bulk electrolysis was performed at 15°C, the mass balance fell to 90% after 30% conversion, whereas at 45°C the mass balance fell to 90% after only 15% conversion. Likewise, after 35% conversion at 45°C, the mass balance was 83%. It is important to note that time plays a role when comparing different experiments as longer times are detrimental to mass balance due to increased duration for homogeneous furanic side reactions<sup>8, 25, 27</sup>, however despite being run for longer durations and reaching similar conversions, the lower temperature experiment still had higher mass balance closures, shown in Figure 2c. These results show that increasing temperature increases the homogeneous side reactions. Furthermore, Figure S5 shows catholytes at similar conversion have an orange color when it was run at 45°C but remains pale yellow when it was run at 15°C indicating that the color change was due to increased temperature rather than conversion.

The selectivities of the parallel reactions to FA and MF are shown in Figure 3a. The selectivity towards MF decreased with an increase in temperature, from 63.3% at 15°C to 39.6% at 45°C.

The selectivity towards FA decreased from 14.6% at 15°C to 9.5% at 45°C. These findings showed that although the conversion increased with temperature, the furanic side reactions were promoted which led to lower selectivities at the higher temperatures. The decrease in selectivity with increasing temperature supports the evidence shown above that the furanic side reactions are promoted by increases in temperature. The trends in Faradaic efficiency to FA and MF showed similar trends, as shown in Figure S6. The Faradaic efficiency to MF showed a decrease from 52.1% at 15°C to 39.5% at 45°C and the Faradaic efficiency to FA increased from 6.0% at 15°C to 7.0% at 25°C before decreasing to 4.7% at 45°C. Overall, the Faradaic efficiency was negatively impacted by an increase in the temperature. This could be due to a combination of an increase in the rate of HER and furanic side reactions consuming FA or MF to undesirable products that are not detected via GCMS.

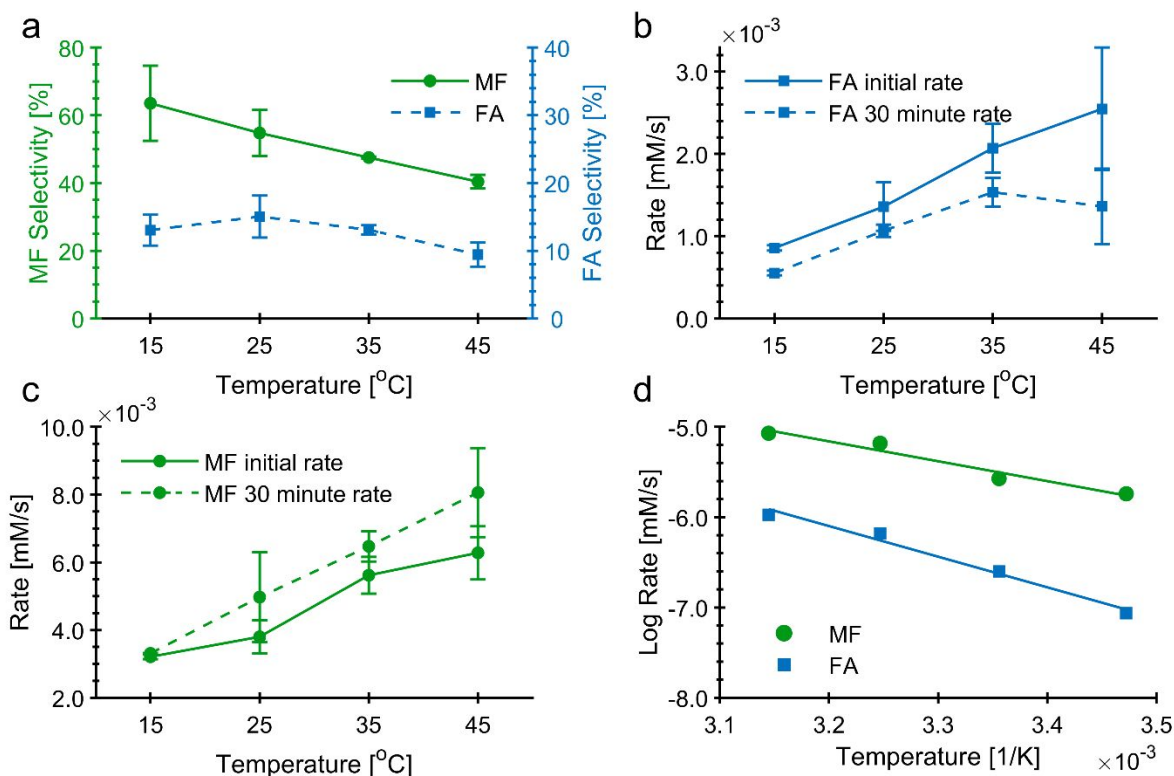


Figure 3. (a) The selectivity for MF and FA from ECH of FF between 15°C and 45°C. (b,c) Rates of the FF to (b) FA and (c) MF reactions between 15°C and 45°C. (d) Arrhenius plot for FA and MF using initial production rates. Conditions: 30 minutes of electrolysis, 100 mM FF initial concentration, -0.560 V vs RHE, 80:20 v:v DI water to acetonitrile with 0.5 M H<sub>2</sub>SO<sub>4</sub>. Conversions, selectivity, Faradaic efficiency, mass balance, rate, and average current density data can be found in Table S3.

The reaction rates of the parallel reactions can also provide insights into the kinetics with respect to temperature and time of electrolysis. The production rates were calculated throughout the experiment to find the initial rate and the rate at 30 minutes. The initial rate and the rate at 30 minutes are shown in Figure 3b and Figure 3c. The initial production rate of FA was shown to increase with temperature, however at 30 minutes the rate decreased as temperature increased from 35°C to 45°C. The decrease in production rate of FA can be attributed to the non-electrochemical side reactions consuming FA as discussed above. The decrease in rate at higher temperatures due to furanic side reactions was not seen in the initial rate because there was insufficient concentration of FA or MF, as the furanic side reactions are concentration dependant<sup>27</sup>. The MF production rate was found to increase with an increase in temperature,

even when increased to 45°C which differs from what was seen with FA. Due to its high volatility, MF evaporates from the catholyte and is carried to the solvent trap with the N<sub>2</sub> purge gas where it is captured. Thus, the majority of MF was separated from the acidic conditions in the catholyte and a decrease in MF production rate due to further side reactions was not observed.

Figure 3d are the Arrhenius plots based on the initial rates for FA and MF. The activation energies of MF and FA across the temperature range studied were (18.3 ± 2.7) kJ/mol and (28.2 ± 2.6) kJ/mol, respectively. It is important to note that the activation energy for electrochemical reactions is also known to be potential dependant<sup>35, 36</sup>, so the findings here are valid only at a potential of -0.56V vs RHE. Based on the higher activation energy required to form FA, FA production should increase with temperature increases, however the results regarding mass balance closures show that the temperature should not be elevated too much as it would promote the homogeneous FA side reactions. Likewise, MF showed a linear increase in selectivity when the electrolysis was run at lower temperatures between the experimental range of 45°C to 15°C. Although further decreases to the temperature could therefore increase the selectivity to MF the production rate will also decrease which in the case of targeting MF is undesirable.

#### **Impact of FF Concentration:**

In addition to the applied potential and temperature, the concentration of FF also impacted the kinetics. To determine the effect that the concentration of FF had on the system, experiments were done at -0.560 V vs RHE and 25°C with initial concentrations of FF between 10 mM and 120 mM in a 80:20 DI water:acetonitrile cosolvent with 0.5 M and 0.1 M H<sub>2</sub>SO<sub>4</sub>. Figure 4a and Figure 4b show the impact that initial concentration had on the selectivity and Faradaic efficiency of the products with 0.5 M H<sub>2</sub>SO<sub>4</sub>. The Faradaic efficiency for both products increased when the starting concentration increased from 10mM to 60mM at which point further increases in concentration gave diminished returns as the Faradaic efficiency plateaued. The Faradaic efficiency to FA and MF is set by the competition of FF ECH and HER, with FF ECH becoming more likely as FF coverage increases, hence increasing the Faradaic efficiency to FA and MF<sup>27</sup>. There is also the presence of side reactions that consume electrons, which will decrease the Faradaic efficiency towards FA and MF<sup>25, 27</sup>. We have shown previously that the Faradaic efficiency to HER and ECH is not impacted significantly when the concentration is further

increased from 100mM to 200mM of FF<sup>27</sup>. The selectivity for the products varied throughout the range of concentration, generally within the standard deviation for the experiments, resulting no significant trend being observed. This shows that the concentration of FF should be higher to promote electron efficiency since there is no significant impact onto the product selectivity.

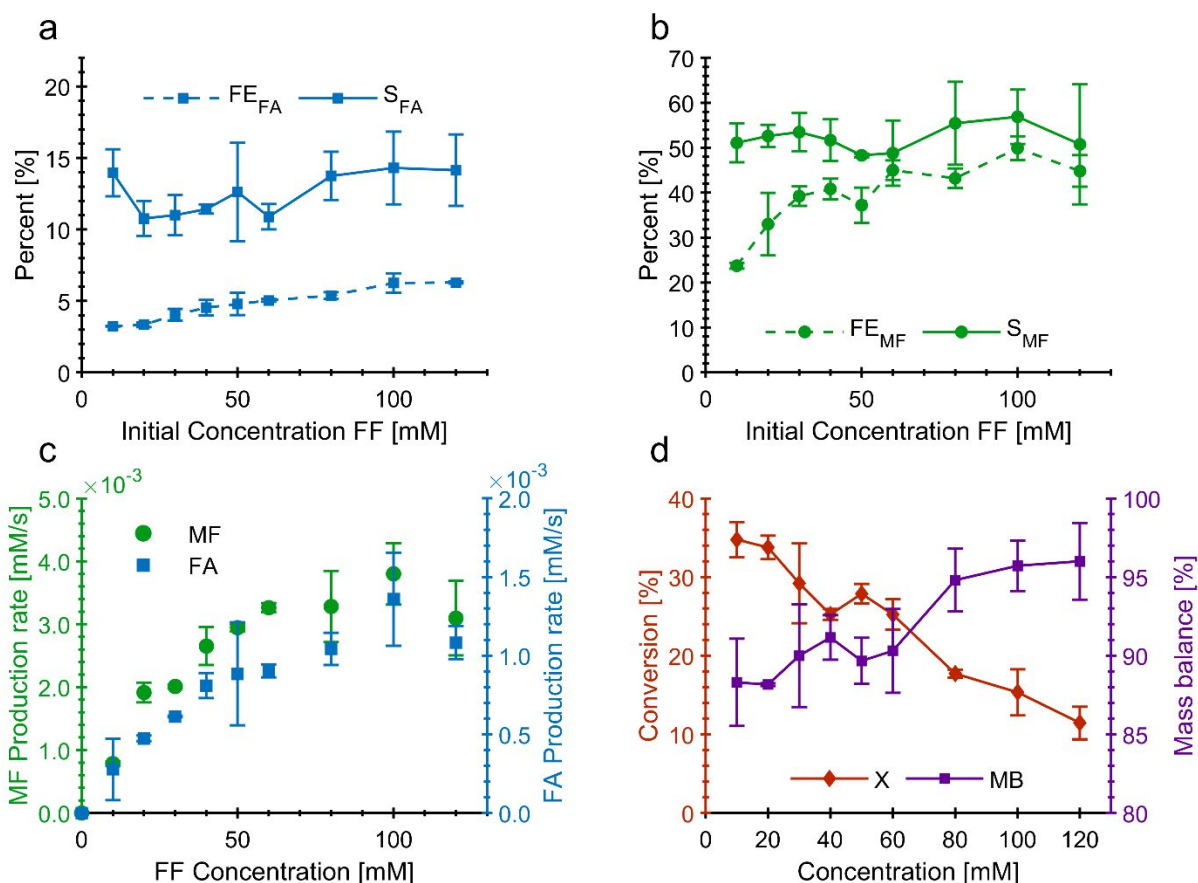


Figure 4. The Faradaic efficiency and selectivity towards (a) FA and (b) MF. (c) The production rates of FF and MF from the ECH of FF. (d) The conversion and mass balance closure from FF ECH. Conditions: 10 to 120 mM concentration of FF, 25°C, -0.560 V vs RHE, 80:20 v:v DI water to acetonitrile with 0.5 M  $H_2SO_4$ . Conversions, selectivity, Faradaic efficiency, mass balance, rate, and average current density data can be found in Table S4.

The production rate of both products as a function of initial concentration of FF in 0.5 M  $H_2SO_4$  is shown in Figure 4c. The production rates for both products in 0.1 M  $H_2SO_4$  is shown in Figure S7. Conversions, selectivity, Faradaic efficiency, mass balance, rate, and average current density data for ECH in 0.1M  $H_2SO_4$  can be found in Table S5. A positive order dependence is

observed for FA and MF between 10 and 80 mM concentrations in both 0.5M H<sub>2</sub>SO<sub>4</sub> and 0.1M H<sub>2</sub>SO<sub>4</sub>. The production rate data in Figures 4c and S7c suggested first order dependence between the production rates of FA and MF to the concentration of FF. Fitting first order rate laws between 0 and 40mM for the data showed R<sup>2</sup> of 0.944 and 0.986 for MF and FA at pH0, and 0.912 and 0.703 for MF and FA at pH1. Further increases to the FF initial concentration show a change to a reaction rate that is zero order with respect to FF initial concentration, denoted by a plateau in the production rate. While in 0.1M H<sub>2</sub>SO<sub>4</sub>, a similar trend is seen with FF concentration, the rate to MF is significantly lower than in 0.5M H<sub>2</sub>SO<sub>4</sub> while the rate to FA is similar to that in 0.5M H<sub>2</sub>SO<sub>4</sub>. This shows that the production of MF depends more significantly on the proton concentration than the production of FA does. The conversion in 0.5M H<sub>2</sub>SO<sub>4</sub> (Figure 4d) decreased with increase in concentration of FF because at higher concentrations a rate that is independent of concentration will give a lower conversion due to the total amount of material. The mass balance in 0.5M H<sub>2</sub>SO<sub>4</sub> has the opposite relationship with concentration, but is correlated with conversion. At higher concentrations of FF, the mass loss is a smaller portion of the total furanics in solution. The conversion and mass balance as a function of FF initial concentration can be seen in Figure 4d.

### Evaluation of FF ECH Reaction Mechanism:

In a recent study by Lopez-Ruiz et al., the kinetics of ECH of benzaldehyde was studied on Pd catalysts<sup>37</sup>. The authors derived several possible reaction mechanisms for ECH of benzaldehyde on Pd between -0.65 V to -1.15 V vs Ag/AgCl and 20 to 180 mM of benzaldehyde. They found that a non-competitive Langmuir-Hinshelwood (NCLH) or an Eley-Rideal (ER) mechanism could match results observed. Due to the absence of hydrogen evolution observed at the conditions studied, a Langmuir-Hinshelwood mechanism was deemed unlikely<sup>37</sup>. They found that HER could be completely suppressed by increasing the concentration of benzaldehyde, showing support for an ER mechanism<sup>37</sup>. In our work on FF ECH, we have seen that HER still occurs when up to 200 mM of FF is present<sup>27</sup>. For this reason, the NCLH mechanism is not ruled out (nor is the ER mechanism).

Several possible mechanistic routes for the ECH of FF to FA and MF were reported in DFT studies by Shan, et al.<sup>38</sup>, of which we began our investigation with. Although the work done by Shan, et al. was primarily done on Ag, Pb, and Ni, they also reported on Cu metal. Figure 5 shows a reaction network for the FF ECH system which labels the intermediates and elementary reactions. Each surface reaction step is labeled with either an F or an M, followed up with a number. The F labels correspond to the surface reactions that lead to FA production

that can be the limiting step while the M labels correspond to surface reactions that can be limiting in MF production. Also shown are the adsorption of FF, and desorption steps of FA and MF. This convention is used to keep track of different combinations of rate limiting steps that can be coupled in a system to produce FA and MF via parallel or series reactions. Using Figure 5 as a guide, different combinations of rate limiting steps were assumed and corresponding rate equations were derived to generate different possible models of the reaction system. We then fit these models to the experimental data to see which were able to capture the kinetics and hence were most likely while ruling out possible models that could not capture the kinetics.

The production rates in 0.5M  $\text{H}_2\text{SO}_4$  and in 0.1M  $\text{H}_2\text{SO}_4$  as function of concentration of FF showed that the reaction order was positive order with respect to FF, but changed to zero order with respect to FF at higher concentrations. This is indicative of a Langmuir-Hinshelwood or Eley-Rideal mechanism. The surface sites could allow for competition between FF and H for sites or could show distinct sites for both FF and H. Mechanisms of Langmuir-Hinshelwood and Eley-Rideal were assumed with either competitive adsorption or non-competitive adsorption to generate our models. In the case of competition for sites, the site was labeled as "S", while in a non-competitive model the distinct sites were labeled "S" for FF sites and "T" for H sites. To keep track of the different possible mechanisms, a naming convention of the limiting steps with the assumed mechanism of competitive Langmuir-Hinshelwood (CLH), NCLH, Eley-Rideal with competitive adsorption (CER) and Eley-Rideal without competitive adsorption (NCER) was used. For example, for the case where F1 is the limiting step for FA production through an NCER mechanism while M7 is limiting for MF production through a NCLH mechanism would be called "F1-NCER, M7-NCLH". Although a combination of LH and ER is possible, a mix of competitive and non-competitive is not as they have conflicting assumptions, and were not evaluated. While Eley-Rideal reactions only have one adsorbed reactant species (FF in our case) and another reactant in the electrolyte (proton in our case) participating in the reaction, CER is used to consider the case of adsorbed hydrogen participating in HER, not ECH, though still competing for active sites for FF.



and MF for the F1-NCLH, M7-NCLH model were 2.95 and 1.32, respectively, which are considered values for good fits. To address the unequal variances in the data, we have also included these equal variance hypothetical reduced chi-squares in the Tables, indicated by the “14.2” subscript.

Table 1. Elementary steps, derived rate equations, and rate constants for the M7-NCLH, F1-NCLH case.

Model	F1-NCLH M7-NCLH
Adsorption reactions	( $K_1$ ): $H^+ + e^- + T \rightleftharpoons H \cdot T$ ( $K_2$ ): $FF + S \rightleftharpoons FF \cdot S$
Elementary Reactions FA	( $k_{rdsFA}$ ): $FF \cdot S + H \cdot T \rightarrow (fur-CH_2O) \cdot S + T$ ( $k_{rdsFA}$ ): $(fur-CH_2O) \cdot S + H \cdot T \rightleftharpoons FA \cdot S + T$ $FA \cdot S \rightleftharpoons FA + S$
Elementary Reactions MF	( $K_3$ ): $FF \cdot S + H \cdot T \rightleftharpoons (fur-CHOH) \cdot S + T$ ( $k_{rdsMF}$ ): $(fur-CHOH) \cdot S + H \cdot T \rightarrow (fur-CH) \cdot S + H_2O + T$ ( $k_{rdsMF}$ ): $(fur-CH) \cdot S + 2H \cdot T \rightleftharpoons MF \cdot S + 2T$ $MF \cdot S \rightleftharpoons MF + S$
Rate Equations	$R_{FA} = \frac{k_{RDSFA} K_2 [FF] K_1 \alpha_H}{(1 + K_2 [FF])(1 + K_1 \alpha_H)}$ $R_{MF} = \frac{k_{RDSMF} K_2 [FF] K_3 (K_1)^2 (\alpha_H)^2}{(1 + K_2 [FF]) * (1 + K_1 \alpha_H)^2}$
Reduced chi-square	FA= 134 MF= 17.5 FA <sub>14.2</sub> = 2.95 MF <sub>14.2</sub> = 1.32
Rate Constants	$K_1 = 25.9 \pm 6$ $K_2 = (0.042 \pm 0.02) \text{ 1/mM}$ $k_{RDSFA} = (0.00148 \pm 0.0003) \text{ mM/s}$ $K_3 k_{RDSMF} = (0.00438 \pm 0.0005) \text{ mM/s}$

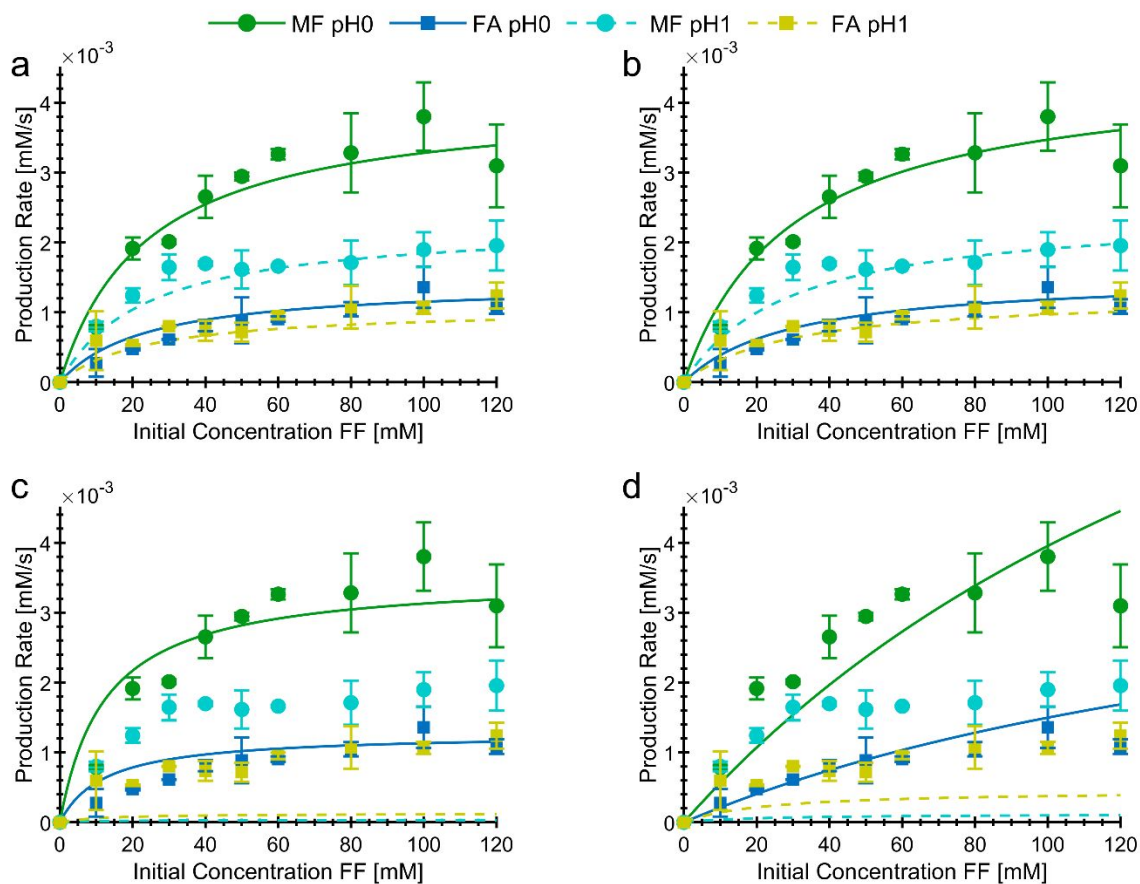


Figure 6. Models assuming MF and FA are produced via different intermediates. All cases show pH 0 and pH 1. Points are experimental data and lines are models fitted to the data. Conditions: 25°C, -0.560 V vs RHE, 80:20 v:v DI water to acetonitrile. (a) F1-NCLH, M7-NCLH are the limiting reactions. (b) F3-NCLH, M4-NCLH are the limiting reactions. (c) F1-NCER, M7-NCER are the limiting reactions. (d) F1-CER, M7-CER are the limiting reactions.

Another case is when the limiting steps for FA and MF are the F3 and M4 steps respectively, both following a NCLH mechanism. Table 2 shows the steps, derived reactions, and rate constants for this scenario. Similar to the F1-NCLH, M7-NCLH case, the constant  $K_1$  value is high such that the proton dependency terms can cancel to show a small impact to the FA rate with change in pH. In this case, a higher proton dependency is present for the MF species which leads to rate constants that provide a slightly higher estimate for the FA production at pH1 than the F1-NCLH, M7-NCLH, which is closer to experimental data shown in Figure 6b. By having a higher proton dependence for the MF reaction (third order for M4-NCLH, second order for M7-NCLH), it is shown that the constant  $K_1$  is much higher (39.8 vs 25.9), which makes the proton terms in the FA reaction closer to canceling out completely. For this reason, we see that a

higher proton dependency for the MF reaction can lead to a closer fit to experimental data for a NCLH reaction to product FA (F1-NCLH or F3-NCLH), however the impact is small. Additionally, the reduced chi-squares were again high for the M4-NCLH, F3-NCLH, as shown in Table 2, however, with a hypothetical error of 14.2% the reduced chi square for FA and MF were 2.04 and 1.21 for FA and MF, respectively.

Table 2. Elementary steps, derived rate equations, and rate constants for the M4-NCLH, F3-NCLH case.

Model	F3-NCLH M4-NCLH
Adsorption reactions	<b>(K<sub>1</sub>)</b> : $H^+ + e^- + T \rightleftharpoons H \cdot T$ <b>(K<sub>2</sub>)</b> : $FF + S \rightleftharpoons FF \cdot S$
Elementary Reactions FA	<b>(k<sub>rdsFA</sub>)</b> : $FF \cdot S + H \cdot T \rightarrow (fur-CHOH) \cdot S + T$ $(fur-CHOH) \cdot S + H \cdot T \rightleftharpoons FA \cdot S + T$ $FA \cdot S \rightleftharpoons FA + S$
Elementary Reactions MF	<b>(K<sub>3</sub>)</b> : $FF \cdot S + H \cdot T \rightleftharpoons (fur-CH_2O) \cdot S + T$ <b>(k<sub>rdsMF</sub>)</b> : $(fur-CH_2O) \cdot S + 2 H \cdot T \rightarrow (fur-CH_2) \cdot S + H_2O + 2T$ $(fur-CH_2) \cdot S + H \cdot T \rightleftharpoons MF \cdot S + T$ $MF \cdot S \rightleftharpoons MF + S$
Rate Equations	$R_{FA} = \frac{k_{RDSFA} K_2 [FF] K_1 \alpha_H}{(1 + K_2 [FF])(1 + K_1 \alpha_H)}$ $R_{MF} = \frac{k_{RDSMF} K_2 [FF] K_3 (K_1)^3 (\alpha_H)^3}{(1 + K_2 [FF]) * (1 + K_1 \alpha_H)^3}$
Reduced chi-square	FA= 96.3 MF= 14.4 FA <sub>14.2</sub> = 2.04 MF <sub>14.2</sub> = 1.21
Rate Constants	K <sub>1</sub> = 39.8 ± 7 K <sub>2</sub> = (0.034 ± 0.01) 1/mM k <sub>RDSFA</sub> = (0.00157 ± 0.0003) mM/s K <sub>3</sub> k <sub>RDSMF</sub> = (0.00485 ± 0.0005) mM/s

The models alone cannot rule out the F1-NCLH, M7-NCLH or the F3-NCLH, M4-NCLH combinations, which both appear as likely combinations of mechanisms. Although the F3-NCLH, M4-NCLH model has a fit that is closer to the mean values of the experimental FA rate at pH1 both the F1-NCLH, M7-NCLH and the F3-NCLH, M4-NCLH combinations are able to describe the data well. The F1-NCLH, M7-NCLH combination, however, has a lower energy barrier to overcome for the M7 step (C-O cleavage) over copper, based on DFT results from Shan et al.<sup>38</sup>, than that of the M4 step in the F3-NCLH, M4-NCLH combination. In addition, our work probing the reactions via applied potential shows that the FA and MF reactions could

proceed via similar reactions due to the similar Tafel slopes which provides support of the F1-NCLH, M7-NCLH combination.

A CLH mechanism was unlikely as our data did not suggest competition for sites as the reaction rates to FA and MF do not decrease at higher initial concentrations of FF, which would be expected if no protons could adsorb to the surface due to high FF coverage. The derived equations for CLH were also unable to model the kinetics of the experimental data. An example of a CLH (F1-CLH, M1-CLH) is shown in Figure S9, where it is seen that the pH 0 curves do not begin to decrease in rate by 120 mM FF, while the pH 1 curves decrease in rate rapidly while the experimental data plateaus. In addition, adsorption-limited and desorption-limited steps were considered but could not fit the data. Adsorption limited kinetics for FA production can be seen in Figure S10, while desorption limited kinetics is not concentration dependent and is not shown. Previous works have shown that when FA is the starting material, in lieu of FF, that electrolysis in 0.5 M H<sub>2</sub>SO<sub>4</sub> over Cu electrodes does not produce MF<sup>23, 27</sup>. This suggests that FA is not an intermediate in the production of MF. Despite being unlikely that a series reaction scheme is followed based upon experimental evidence, the equations are derived and results can also be seen in the supplemental information.

When a NCER mechanism was assumed, the dependence on the proton led to a major underestimate of the reaction rates for MF and FA at pH1. This can be seen in the case of F1-NCER, M7-NCER, shown in Figure 6c. The equations and rate constants for this case (F1-NCER, M7-NCER) are in Table S6. When a case with mixed NCLH and NCER was assumed, for example F1-NCLH, M7-NCER, the product which proceeds via an NCER mechanism (In this case MF) would underestimate the rate at pH1, shown in Figure S11. The case in which FA production proceeds via a NCER mechanism, F1-NCER, M7-NCLH, is shown in Figure S12.

When a case of competition for sites between protons and FF is assumed where both products are formed via a CER mechanism with competitive adsorption it is found that the rate model does not plateau for either product at pH0 and remains very low (underestimate) for both products at pH1. An example of this case (F1-CER, M7-CER) is shown in Figure 6d. Although the M9 route to MF can provide a good fit, ECH of FA is not observed experimentally<sup>23, 27</sup> and hence is ruled out. The M1-NCLH route for MF production has a fit similar to that of the M7-NCLH case but the  $k_{RDSMF}$  depends on  $K_3$  for the M7-NCLH case, however the C-O cleavage step directly from FF was found to have a much higher energy barrier from DFT<sup>38</sup>, and is unlikely.

This work has shown that the ECH of FF follows NCLH mechanisms for both FA and MF production. The FA is likely limited by either the step F1 or step F3, showing a first order dependence on the proton. The MF is likely limited by the M7 or the M4 step.

### **Conclusions:**

This work investigated the competition between FA and MF production from ECH of FF in acidic electrolytes over Cu. The kinetics were probed using the concentration of FF, the applied potential, and the temperature of the ECH and insights into the mechanism were provided.

The production of FA and MF from FF on Cu followed Butler-Volmer kinetics. Increasing temperature led to increased initial production rate. The temperature increase also increased the rate of side reactions which consumed FA and had the most significant impact at 45°C where the reaction rate of FA was lower at 30 minutes of ECH compared to 35°C. Varying the initial FF concentration showed that the rate for both FA and MF depends on the concentration of FF, which is positive order at low concentrations of FF and plateaus to a zero order at higher concentrations of FF. Eley-Rideal and Langmuir-Hinshelwood mechanisms were proposed and models were fit to the data, however only the models where FA and MF were both produced via a NCLH mechanism were able to capture the kinetics of the experimental data, whereas ER mechanisms would significantly underestimate the rate of FA and MF at pH1.

A first order dependence on proton for FA was found to match experimental data at pH0 and pH1 while a second order dependence on proton for FA underestimated the rate at pH 1. This shows that FA production is likely limited by the first surface reaction of FF. For MF production, the models provided here cannot decipher between all of the possible rate limiting steps. Previous work has showed that C-O cleavage is likely the limiting step in MF production due to the high energy barrier required. A model with MF production via the C-O cleavage through a M4 or M7 rate limiting step can fit the experimental data closely. Two cases that are more likely are the F1-NCLH, M7-NCLH and the F3-NCLH, M4-NCLH. Although the M4 step in the F3-NCLH, M4-NCLH can provide a closer fit to experimental data, the M7 step in the F1-NCLH, M7-NCLH has a lower energy barrier and Tafel analysis shows evidence of having the same number of electrons in the rate limiting step, which is true for the F1-NCLH, M7-NCLH case. Therefore, it is likely that the rate limiting steps in FF ECH are the F1 hydrogenation step through the  $C_4H_3O-CH_2O$  intermediate to form FA, and the M7 C-O cleavage step of the  $C_4H_3O-CHOH$  intermediate to form MF.

**Conflicts of interest:**

The authors declare no conflicts of interest for this work.

**Author Information:****Corresponding Author**

**Elizabeth J. Biddinger** – Department of Chemical Engineering,  
The City College of New York, New York, New York 10031,  
United States;

\*E-mail: ebiddinger@ccny.cuny.edu. Tel.: (+1) 212-650-6323.

ORCID: 0000-0003-3616-1108

**Author**

**Andrew S. May** – Department of Chemical Engineering,  
The City College of New York, New York, New York 10031,  
United States;

ORCID: 0000-0001-7780-2907

**Author**

**Steven M. Watt** – Ph.D. Program in Chemistry,  
The Graduate Center of the City University of New York, New York, New York 10016,  
United States;

Department of Chemical Engineering,  
The City College of New York, New York, New York 10031,  
United States

ORCID: 0000-0002-6198-1127

**Acknowledgments:**

This research was supported by the U.S. Department of Energy, Office of Science, Office of Basic Energy Sciences, Catalysis Science program, under Award DE-SC0019134.

### Footnotes:

Electronic supplementary information is available.

### References:

1. D. M. Alonso, J. Q. Bond and J. A. Dumesic, *Green Chem.*, 2010, **12**, 1493-1513.
2. D. C. Elliott, *Energy Fuels*, 2007, **21**, 1792-1815.
3. C. H. Lam, W. Deng, L. Lang, X. Jin, X. Hu and Y. Wang, *Energy Fuels*, 2020, **34**, 7915-7928.
4. S. A. Akhade, N. Singh, O. Y. Gutiérrez, J. Lopez-Ruiz, H. Wang, J. D. Holladay, Y. Liu, A. Karkamkar, R. S. Weber, A. B. Padmaperuma, M.-S. Lee, G. A. Whyatt, M. Elliott, J. E. Holladay, J. L. Male, J. A. Lercher, R. Rousseau and V.-A. Glezakou, *Chem. Rev.*, 2020, **120**, 11370–11419.
5. S. Kim, E. E. Kwon, Y. T. Kim, S. Jung, H. J. Kim, G. W. Huber and J. Lee, *Green Chem.*, 2019, **21**, 3715-3743.
6. Y. Kwon, K. J. P. Schouten, J. C. van der Waal, E. de Jong and M. T. M. Koper, *ACS Catal.*, 2016, **6**, 6704-6717.
7. S. Chen, R. Wojcieszak, F. Dumeignil, E. Marceau and S. Royer, *Chem. Rev.*, 2018, **118**, 11023-11117.
8. A. S. May and E. J. Biddinger, *ACS Catal.*, 2020, **10**, 3212-3221.
9. T. Werpy and G. Petersen, *Top value added chemicals from biomass: I. Results of screening for potential candidates from sugars and synthesis gas*, United States, 2004.
10. K. J. Zeitsch, *The chemistry and technology of furfural and its many by-products*, Elsevier, 2000.
11. C. Wang, H. Xu, R. Daniel, A. Ghafourian, J. M. Herreros, S. Shuai and X. Ma, *Fuel*, 2013, **103**, 200-211.
12. H. E. Hoydonckx, W. M. Rhijn, W. Van Rhijn, D. De Vos and J. Pierre, *Furfural and Derivatives*, Wiley-VCH Verlag GmbH & Co. KGaA, Weinheim, 2012.
13. W. C. Albert and A. Lowy, *T. Electrochem. Soc.*, 1939, **75**, 367-375.
14. P. Nilges and U. Schröder, *Energy Environ. Sci.*, 2013, **6**, 2925-2931.
15. S. K. Green, J. Lee, H. J. Kim, G. A. Tompsett, W. B. Kim and G. W. Huber, *Green Chem.*, 2013, **15**, 1869-1879.
16. Y. Cao, J. Knijff, A. Delparish, M. F. N. d'Angelo and T. Noël, *ChemSusChem*, 2020, **14**, 590-594.
17. U. Sanyal, K. Koh, L. C. Meyer, A. Karkamkar and O. Y. Gutiérrez, *J. Appl. Electrochem.*, 2021, **51**, 27-36.
18. E. Andrews, J. A. Lopez-Ruiz, J. D. Egbert, K. Koh, U. Sanyal, M. Song, D. Li, A. J. Karkamkar, M. A. Derewinski, J. Holladay, O. Y. Gutiérrez and J. D. Holladay, *ACS Sustainable Chem. Eng.*, 2020, **8**, 4407-4418.
19. J. A. Lopez-Ruiz, E. Andrews, S. A. Akhade, M.-S. Lee, K. Koh, U. Sanyal, S. F. Yuk, A. J. Karkamkar, M. A. Derewinski, J. Holladay, V.-A. Glezakou, R. Rousseau, O. Y. Gutiérrez and J. D. Holladay, *ACS Catal.*, 2019, **9**, 9964-9972.
20. P. Parpot, A. P. Bettencourt, G. Chamoulaud, K. B. Kokoh and E. M. Belgsir, *Electrochim. Acta*, 2004, **49**, 397-403.
21. S. Jung, A. N. Karaiskakis and E. J. Biddinger, *Catal. Today*, 2019, **323**, 26-34.

22. Z. Li, S. Kelkar, C. H. Lam, K. Luczek, J. E. Jackson, D. J. Miller and C. M. Saffron, *Electrochim. Acta*, 2012, **64**, 87-93.
23. X. H. Chadderdon, D. J. Chadderdon, J. E. Matthiesen, Y. Qiu, J. M. Carraher, J.-P. Tessonnier and W. Li, *J. Am. Chem. Soc.*, 2017, **139**, 14120-14128.
24. Y. Cao and T. Noël, *Org. Process Res. Dev.*, 2019, **23**, 403-408.
25. S. Jung and E. J. Biddinger, *ACS Sustainable Chem. Eng.*, 2016, **4**, 6500-6508.
26. R. Bababrik, D. Santhanaraj, D. E. Resasco and B. Wang, *J. Appl. Electrochem.*, 2021, **51**, 19-26.
27. S. Jung and E. J. Biddinger, *Energy Technol.*, 2018, **6**, 1370-1379.
28. R. W. Revie and H. H. Uhlig, *Corrosion and Corrosion Control: An Introduction to Corrosion Science and Engineering*, John Wiley & Sons, Inc., New Jersey, 4th Ed. edn., 2008.
29. J. R. McKone, S. C. Marinescu, B. S. Brunshwig, J. R. Winkler and H. B. Gray, *Chem. Sci.*, 2014, **5**, 865-878.
30. R. M. Bullock, *Chem*, 2017, **2**, 444-446.
31. M. Zeng and Y. Li, *J. Mater. Chem. A*, 2015, **3**, 14942-14962.
32. *Nature Catalysis*, 2019, **2**, 735-735.
33. L. Liu, H. Liu, W. Huang, Y. He, W. Zhang, C. Wang and H. Lin, *J. Electroanal. Chem.*, 2017, **804**, 248-253.
34. T. Shinagawa, A. T. Garcia-Esparza and K. Takanahe, *Scientific Reports*, 2015, **5**, 13801.
35. U. Sanyal, Y. Song, N. Singh, J. L. Fulton, J. Herranz, A. Jentys, O. Y. Gutiérrez and J. A. Lercher, *ChemCatChem*, 2019, **11**, 575-582.
36. A. J. Bard and L. R. Faulkner, *Electrochemical methods: fundamentals and applications*, John Wiley & Sons, New York, 2001.
37. J. A. Lopez-Ruiz, U. Sanyal, J. Egbert, O. Y. Gutiérrez and J. Holladay, *ACS Sustainable Chem. Eng.*, 2018, **6**, 16073-16085.
38. N. Shan, M. K. Hanchett and B. Liu, *J. Phys. Chem. C*, 2017, **121**, 25768-25777.